Molecular Biology of the Cell
Vol. 20, 4335–4347, October 15, 2009

Organization and Dynamics of the *Aspergillus nidulans* Golgi during Apical Extension and Mitosis

Areti Pantazopoulou and Miguel A. Peñalva

Departamento de Microbiología Molecular, Centro de Investigaciones Biológicas C.S.I.C., Madrid 28040, Spain

Submitted March 30, 2009; Revised July 31, 2009; Accepted August 11, 2009
Monitoring Editor: Sean Munro

Aspergillus nidulans **hyphae grow exclusively by apical extension. Golgi equivalents (GEs) labeled with mRFP-tagged PH^{OSBP} domain form a markedly polarized, dynamic network of ring-shaped and fenestrated cisternae that remains intact during "closed" mitosis. mRFP-PH^{OSBP} GEs advance associated with the growing apex where secretion predominates but do not undergo long-distance movement toward the tip that could account for their polarization. mRFP-PH^{OSBP} GEs overlap with the *trans*-Golgi resident Sec7 but do not colocalize with also polarized accretions of the early Golgi marker $GrhA^{Grh1}$-GFP, indicating that early and late Golgi membranes segregate spatially. AnSec23-GFP ER exit sites (ERES) are numerous, relatively static foci localizing across the entire cell. However, their density is greatest near the tip, correlating with predominance of early and *trans*-Golgi elements in this region. Whereas GrhA-GFP structures and ERES reach the apical dome, mRFP-PH^{OSBP} GEs are excluded from this region, which contains the endosome dynein loading zone. After latrunculin-mediated F-actin disruption, mRFP-PH^{OSBP} GEs fragment and, like AnSec23-GFP ERES, depolarize. Brefeldin A transiently collapses late and early GEs into distinct aggregates containing Sec7/mRFP-PH^{OSBP} and GrhA-GFP, respectively, temporarily arresting apical extension. Rapid growth reinitiates after washout, correlating with reacquisition of the normal Golgi organization that, we conclude, is required for apical extension.**

INTRODUCTION

Hyphal cells of filamentous fungi grow exclusively by apical extension (Momany, 2002). In *Aspergillus nidulans* cells are multinucleated, but the different nuclei are evenly spaced across the entire length of the cell. Hence intracellular distances between nuclei or between the growing apexes and distal parts of the tip cells may be notably large. Thus, it should come as no surprise that the localization of the machinery or membrane organelles specialized in a given process reflects, at the subcellular level, the site(s) where their function is mainly required.

Endocytosis and secretion show specialized subcellular distribution in hyphae. Studies with the plasma membrane t-SNARE SsoA and the exocyst component $SecC^{Sec3}$ established that, in agreement with EM analyses (Harris *et al*., 2005; Hohmann-Marriott *et al*., 2006), secretion predominates at the apexes (Taheri-Talesh *et al*., 2008); (as in this article, we shall differentiate the growing extreme of the hypha [the tip] from the apex ["the tip of the tip"]). Endocytosis can occur elsewhere, but predominates in a subapical ring mediating the endocytic recycling of the v-SNARE SynA (Valdez-Taubas and Pelham, 2003; Taheri-Talesh *et al*., 2008), hypothetically facilitating the endocytic removal of the excess of materials delivered to the apical dome by exocytosis (Taheri-Talesh *et al*., 2008; Upadhyay and Shaw, 2008; Lee *et al*., 2008; Araujo-Bazán *et al*., 2008b; Higuchi *et al*., 2009).

Hyphal cells have specialized mechanisms ensuring intracellular communication. For example, in *Ustilago maydis* and *A. nidulans*, early endosomes show long-distance, bidirectional movement on microtubules (MTs), trafficking through the hyphal tip (where MTs are oriented with their plus ends toward the apex) before undergoing dynein-dependent retrograde movement (Wedlich-Soldner *et al*., 2002; Peñalva, 2005; Fuchs *et al*., 2006; Steinberg, 2007; Galindo *et al*., 2007; Zekert and Fischer, 2008; Abenza *et al*., 2009). Functional impairment of dynein prevents this retrograde movement, resulting in an exaggerated endosomal compartment in the tip (the NudA compartment). Thus, the hyphal tip region containing the apex, where exocytosis predominates, the subapical endocytic ring, where endocytosis is most active, and the dynein loading zone for early endosomes, plays a key role in the biology of the hyphal tip cell. The Spitzenkörper (SPK) is a dense meshwork of secretory vesicles and actin filaments located in the apex, underneath the plasma membrane (Harris *et al*., 2005; Hohmann-Marriott *et al*., 2006; Taheri-Talesh *et al*., 2008). Functionally the SPK is a microfilament organizing center from which actin cables radiate (Pearson *et al*., 2004; Taheri-Talesh *et al*., 2008). In current models, these cables mediate the short range delivery of secretory vesicles to the apex, thus playing a key role in maintaining polarized secretion and exocytosis.

EM studies have shown that the Golgi cisternae of filamentous fungi (Howard, 1981; Kurtz *et al*., 1994; Momany, 2002) and *S. cerevisiae* (Rambourg *et al*., 1993; Rambourg *et al*., 1995b; Rambourg *et al*., 2001) do not form the character-

This article was published online ahead of print in *MBC in Press* (http://www.molbiolcell.org/cgi/doi/10.1091/mbc.E09–03–0254) on August 19, 2009.

Address correspondence to: Miguel A. Peñalva (penalva@cib.csic.es).

Abbreviations used: BFA, brefeldin A; F-actin, filamentous polymers of actin; EM, electron microscopy; ER, endoplasmic reticulum; ERES, ER exit sites; GE, Golgi equivalent; GFP, green fluorescent protein; mRFP, monomeric red fluorescent protein; LatB, latrunculin B; MT(s), microtubule(s); NPCs, nuclear pore complexes; PH, pleckstrin homology domain; OSBP, human oxysterol binding protein; PLCδ, rat phospholipase δ1; SPK, Spitzenkörper; UTR, untranslated region.

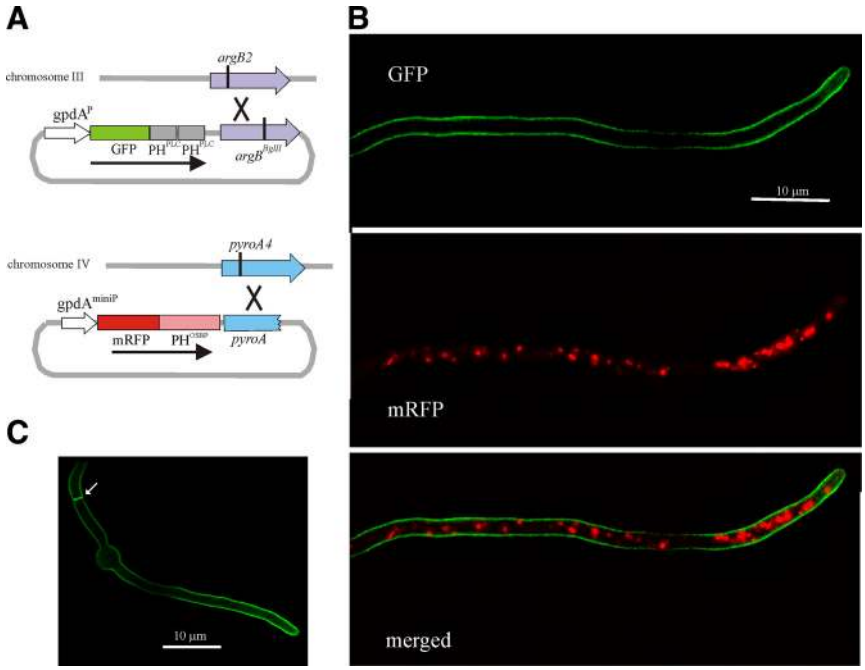

Figure 1. Subcellular localization of PtdIns4,5*P*2 and PtdIns4*P* fluorescent fusion protein probes. (A) Schematic representation of the constructs and strategies used for targeting them to the *pyroA* and *argB* loci. (B) GFP and mRFP channel images correspond to maximal intensity projections of deconvolved z-stacks of a strain coexpressing mRFP-PH^{OSBP} and GFP-(PH$^{PLC\delta}$)$_2$. (C) Maximal intensity projection of a z-stack series of deconvolved images of a strain expressing GFP-(PH$^{PLC\delta}$)$_2$.

istic stacks seen in animal and plant cells, and are instead organized as a network of tubules and fenestrated cisternae, denoted Golgi equivalents (GEs). An important finding was that fluorescently tagged Golgi resident proteins can be used to visualize in vivo the different domains of the *S. cerevisiae* Golgi, which was thoroughly exploited to obtain supporting evidence for the cisternal maturation model (Matsuura-Tokita *et al*., 2006; Losev *et al*., 2006), recently modified by the so-called rapid-partitioning model (Patterson *et al*., 2008; Jackson, 2009).

Recent studies using fluorescently tagged proteins have shown that *A. nidulans* GEs are polarized (Breakspear *et al*., 2007; Hubbard and Kaminskyj, 2008). However, these studies have not exploited the possibilities that multidimensional epifluorescence microscopy techniques offer to study the in vivo changes undergone by the Golgi, which is a very dynamic compartment continuously undergoing cisternal maturation, nor have they addressed the morphological and domain organization of GEs, their relationship with the transitional ER, the determinants of GE polarization, and their fate during the morphogenetic transition or during mitosis. Thus, we undertook the characterization in vivo of the organization, morphology, and dynamics of the Golgi in growing *A. nidulans* hyphae using fluorescent protein–tagged reporters of ER exit sites (ERES), early and late Golgi membrane domains. We addressed the spatial segregation of these domains and the cytoskeletal dependence of the polarization of late Golgi cisternae, which predominate in the region located between the leading nucleus and the growing apex, correlating with polarization of the early Golgi and ERES. The Golgi organization is disrupted by brefeldin A.

MATERIALS AND METHODS

Molecular Genetic Manipulations

The *gpdA^{mini}* promoter plasmid pgpd003, based on *gpdA^{mini}*, an attenuated version of the glyceraldehyde 3-phosphate dehydrogenase (*gpdA*) promoter, was designed to express mRFP-PH^{OSBP} at moderately high levels. This vector integrates into the chromosome IV *pyroA* locus by a single cross-over (see Figure 1A). Transformants carrying single-copy integration events were identified after Southern analysis. Knowing the precise chromosomal location of the transgene facilitated the construction, using classical genetics, of recombinant mRFP-PH^{OSBP} strains derived from primary transformants. This construct drives expression of full-length mRFP-PH^{OSBP}, as determined by Western blots (data not shown).

The pleckstrin homology domain of the human oxysterol binding protein (PH^{OSBP}) was PCR-amplified (primers 3 and 4, Supplemental Table S1), N-terminally tagged with mRFP, and cloned into pgpdA003 to yield p1793. Briefly, the vector contains a NcoI-HindIII-EcoRI-XmaI polylinker, which is flanked upstream of the NcoI site by 352 bps of the *A. nidulans gpdA* (glyceraldehyde 3-phosphate dehydrogenase) promoter region, and downstream of the XmaI site by a 212-bp fragment of the *gpdA* 3′-UTR containing the polyadenylation site. The plasmid additionally includes a C-terminally–truncated *A. nidulans pyroA* gene (as SpeI-EagI), which targets integration into the *pyroA* locus of strains carrying the pyridoxine auxotrophy mutation *pyroA4* (Calcagno-Pizarelli *et al*., 2007).

The tandemly repeated PH domain of rat phospholipase C 1 (PLCδ) (Stefan *et al*., 2002) was PCR amplified (primers 11 and 12), N-terminally tagged with GFP (GFP-2xPLCδ), and expressed from a second expression vector, denoted pgpd-argB. Unlike pgpd003, pgpd-argB carries the complete *gpdA* promoter (Punt *et al*., 1990), thus driving high levels of expression. pgpd-argB contains an *argB^{BglII}* allele which targets integration into the chromosome III *argB* locus of strains carrying the *argB2* mutation (Mingot *et al*., 1999).

HypB^{Sec7}, AnSec23, and GrhA were C-terminally tagged with GFP after homologous-recombination–mediated replacement of the resident *hypB^{SEC7}*, *Ansec23*, and *grhA* genes by linear fusion PCR products, as described (Yang *et al*., 2008). *hypB^{SEC7}-gfp*, *Ansec23-gfp*, and *grhA-gfp* drive expression, under the control of the respective physiological promoters, of the corresponding fusion proteins, in which the GFP tag is separated from the respective C termini by a (Gly-Ala)5 linker peptide (Szewczyk *et al*., 2006). cDNA database sequence coverage confirmed that the in silico predictions of the C termini of AnSec23 and GrhA in the *A. nidulans* genome database are correct.

Aspergillus *Techniques*

A. nidulans strains carried markers in standard use (Clutterbuck, 1993; See also http://www.gla.ac.uk/ibls/molgen/aspergillus/index.html). Standard genetic techniques were used throughout. Strains used in this work are detailed in Supplemental Table S2. Constructs and PCR products were integrated into the genome after transformation (Tilburn *et al*., 1983). Integration events were in all cases verified by Southern analysis. PCR-derived constructs were sequenced to confirm the absence of thermostable polymerase-induced mutations.

Image Acquisition

For all microscopy experiments, *A. nidulans* cells were cultured in "watch minimal medium" (WMM; Peñalva, 2005), using an incubation temperature of 25 to 27°C unless otherwise indicated.

mRFP-PH^{OSBP}-labeling of GEs was affected by anaerobiosis or mechanical pressure resulting from mounting hyphae on microscopy slides, after which fluorescence became markedly cytoplasmic in <5 min. Thus, fluorescence microscopy experiments were in all cases performed in vivo, using Lab-Tek chambered coverglasses (Nalge Nunc International, Rochester NY) and a PeCon heating insert (PeCon, Erbach, Germany) driven by a two-channel Leica 37-2 digital temperature controller (Leica Microsystems, Wetzlar, Germany). We used an inverted Leica DMI6000B microscope with motorized z-focus and a Leica EL6000 external light source for epifluorescence excitation, which includes a built-in excitation shutter. The microscope was driven by Metamorph (Invitrogen, Carlsbad, CA) software using a DMI6000-specific driver. Images were acquired using HCX ×63 1.4 numerical aperture (NA) or ×100 1.4 NA objectives and a Hamamatsu ORCA ER-II cooled-charge coupled device camera (Hamamatsu Photonics, Massy, France). The microscope was equipped with Semrock Brightline GFP-3035B and TXRED-4040B filter sets (Semrock, Rochester, NY). The fluorescence of the mRFP-PH^{OSBP} Golgi reporter is robust and compatible with relatively low exposure times. However, for time lapse acquisition involving dual wavelength or z-stack series for relatively long time periods (such as those acquired to analyze recovery after drug washout or the fate of the Golgi during mitosis), we additionally used attenuated excitation light in combination with image binning.

In time-lapse experiments showing the absence of colocalization of GrhA-GFP and mRFP-PH^{OSBP} "brefeldin bodies" (Supplemental Movie S11) and the lack of effect of BFA on An Sec23-GFP (which involved coimaging with mRFP-PH^{OSBP} brefeldin bodies, Supplemental Figure S2), we used a DualView DV2 image splitter (Photometrics, Tucson, AZ) optimized for simultaneous two-color imaging of GFP and mRFP.

Image Processing and Statistical Analyses

Image acquisition, kymographs, contrast adjustment, and color combining were made using Metamorph (Invitrogen). Maximal intensity projections were obtained from z-stacks using the Metamorph 3D plugin and, when indicated, were further contrasted using the "sharpening" algorithm. Images were converted to 8-bit greyscale or 24-bit RGB and annotated using Corel Draw before being saved to TIFF. Time-lapse sequences were time-scaled and assembled into movies using appropriate Metamorph plugins and converted to Quicktime movies using ImageJ 1.37 http://rsb.info.nih.gov/ij. When indicated, images were deconvolved using the blind deconvolution algorithms of AutoDeblur software (Autoquant X2, MediaCybernetics, Bethesda, MD).

The polarized distribution of GEs ahead of the leading nucleus was estimated using strain MAD2060 (Supplemental Table S2), expressing mRFP-PH^{OSBP} and GFP-PacC[27]. Maximal intensity projections of z-stacks were used to determine the average fluorescence intensity in regions of interest corresponding to the area between two successive nuclei and between the apex and the leading nucleus. Values were expressed relative to the fluorescence of the latest, which was arbitrarily set as 100%.

To estimate the approximate size of GEs in the presence or absence of latrunculin B we chose GEs in tip regions giving rise to approximately circular structures and manually determined their diameters using background-subtracted images. We measured n = 31 particles (5 untreated hyphae) and n = 52 particles (5 hyphae treated for 1 h with latrunculin).

Statistical analyses were performed using GraphPad Prism 5.00 for Windows (GraphPad Software, San Diego, CA). Consistency of analyzed values with a Gaussian distribution was assessed using the D'Agostino and Pearson test of normality. Statistical significance of observed differences was estimated using the unpaired *t* test (one or two-tailed) for Gaussian distributions or the Mann–Whitney test for non-Gaussian distributions.

Inhibitor Treatments

These were essentially made as described (Taheri-Talesh *et al*., 2008), using pH 6.5 WMM. Hyphae were cultured in incubating chambers for about 16h at 25°C before removing the medium and replacing it with the same amount of prewarmed medium containing the inhibitor or, in control experiments, with an equivalent amount of the stock solution solvent. Inhibitors were removed after four washes with prewarmed WMM.

Brefeldin A (BFA, Fluka, Buchs, Switzerland) was added from a 10 mg/ml stock in DMSO at final concentrations of 100 or 300 μg/ml. Rates of apical extension were determined in germlings that were cultured in the presence of 300 μg/ml BFA or of the corresponding amount of the BFA solvent DMSO for 8 to 9 h at 28°C. Extension rates were determined by measuring the changes in hyphal tip position using Nomarski photographs taken every 2 min over a 10-min time period.

Latrunculin B (LatB) was used as described (Taheri-Talesh *et al*., 2008), at a final concentration of 40 μg/ml (100 μM). The drug was added from a 10 mM stock in DMSO. Hyphae were incubated in the presence of latrunculin B for a maximum period of 45 min, after which the inhibitor was washed out and hyphal tips resumed growth, usually from subapical regions.

Benomyl (Horio and Oakley, 2005) was added at final concentrations of 5 μg/ml (17.2 μM) from a 5 mM stock in ethanol. Hyphae were incubated in the presence of benomyl for a maximum period of 1 h, after which the inhibitor was washed out and hyphal tips resumed growth.

Early Endosome Labeling

Early endosomes were labeled with GFP-RabA^{Rab5} (Abenza *et al*., 2009). To coimage GFP-RabA^{Rab5}early endosomes and mRFP-PH^{OSBP}, MAD2195 and MAD2196 strains (Supplemental Table S2) were cultured at 25°C for ≈14h in WMM supplemented with 0.1% (wt/vol) glucose as sole carbon source (non-inducing conditions for the *alcA^{p}* driving expression of RabA^{Rab5}; Abenza *et al*., 2009) and shifted for 3 to 4 h to the same medium containing 1% ethanol (vol/vol; inducing conditions for the *alcA^{p}*) before microscopic observation.

To determine the spatial relationship of the NudA1 compartment with the most apical GEs, we used *nudA1* or *kinA*Δ mutant strains. *kinA*Δ *alcA^{p}::gfp::rabA^{RAB5} gpdA^{mini}::mrfp::PH^{OSBP}* strains (MAD2120 or MAD2122) were cultured at 25°C and subjected to ethanol induction as above. *nudA1* strains MAD2106 or MAD2107 (*nudA1 alcA^{p}::gfp::rabA^{RAB5} gpdA^{mini}::mrfp::PH^{OSBP}*) (Supplemental Table S2) were cultured at the 25°C permissive temperature for ≈14 h before being shifted to 1% ethanol-WMM for 3 h as described above, and further incubated for an additional 1 to 4 h at 42°C. Appropriate controls expressing each fluorescent fusion protein alone were set up to rule out the possibility of cross-talk between the red and green channels.

RESULTS

mRFP-PH^{OSBP} Localizes to Golgi Equivalents but not to the Plasma Membrane

A previous study used GFP-CopA (CopA encodes α-COP, a component of the COPI coat) to study the *A. nidulans* Golgi (Breakspear *et al*., 2007). The role of COPI vesicles within the Golgi is not fully understood (Béthune *et al*., 2006) and, in *S. cerevisiae*, COPI is present in both early and late GEs (Rossanese *et al*., 2001). As we were particularly interested in the in vivo dynamics of GEs in the context of apical secretion, we constructed a robust *trans*-Golgi-specific reporter. *gpdA^{mini}::mRFP-PH^{OSBP}* encodes a protein consisting of the pleckstrin homology domain of the human oxysterol binding protein (PH^{OSBP}) fused to mRFP. PH^{OSBP} is recruited to the cytosolic face of *trans*-Golgi membranes through the combinatorial recognition of PtIns4P and of the Golgi GTPase Arf1 (Levine and Munro, 2002). This construct, which expresses mRFP-PH^{OSBP} at moderately high levels to minimize exposure times during time-lapse fluorescence microscopy, was targeted to the *pyroA* locus by homologous recombination (Figure 1A). A second transgene encoding a tandem repeat of the human phospholipase δ PH domain (2xPLCδ) fused to GFP was constructed as specificity control because this tandemly repeated domain binds PtdIns4,5*P2* and, in *S. cerevisiae*, localizes exclusively to the plasma membrane (Stefan *et al*., 2002; Levine and Munro, 2002). The GFP-2xPLCδ construct was targeted in single copy to the *argB* locus (Figure 1A). As predicted, GFP-2xPLCδ labels exclusively the plasma membrane (Figure 1, B and C). In contrast, mRFP-PH^{OSBP} (Figure 1B) accumulated instead in intracellular bodies, resembling those that had been visualized with fluorescent versions of proteins predicted to be Golgi residents (Breakspear *et al*., 2007; Hubbard and Kaminskyj, 2008; Jackson-Hayes *et al*., 2008).

Characterization of PtdIns4P-Containing Bodies and Colocalization with Sec7, a Resident Protein of the **trans-***Golgi*

GFP-CopA GEs are "doughnut"-like, spherical, and elongated structures showing polarization toward the apex (Breakspear *et al*., 2007). mRFP-PH^{OSBP} indeed localizes to strongly polarized GEs (Figures 1B and 2A, and see below) also resembling tubules, hollow rings frequently showing tubular extensions and ellipsoids/spheres (Figure 2B). We exploited the robustness of our fluorescent reporter in time-lapse microscopy studies, which revealed that ellipsoid/spherical mRFP-PH^{OSBP} GEs are in fact rings of variable diameters containing accretions of intense fluorescence (Figure 2B, Supplemental Movie S1). mRFP-PH^{OSBP} GEs are interconnected by tubular structures that can be as long as 8

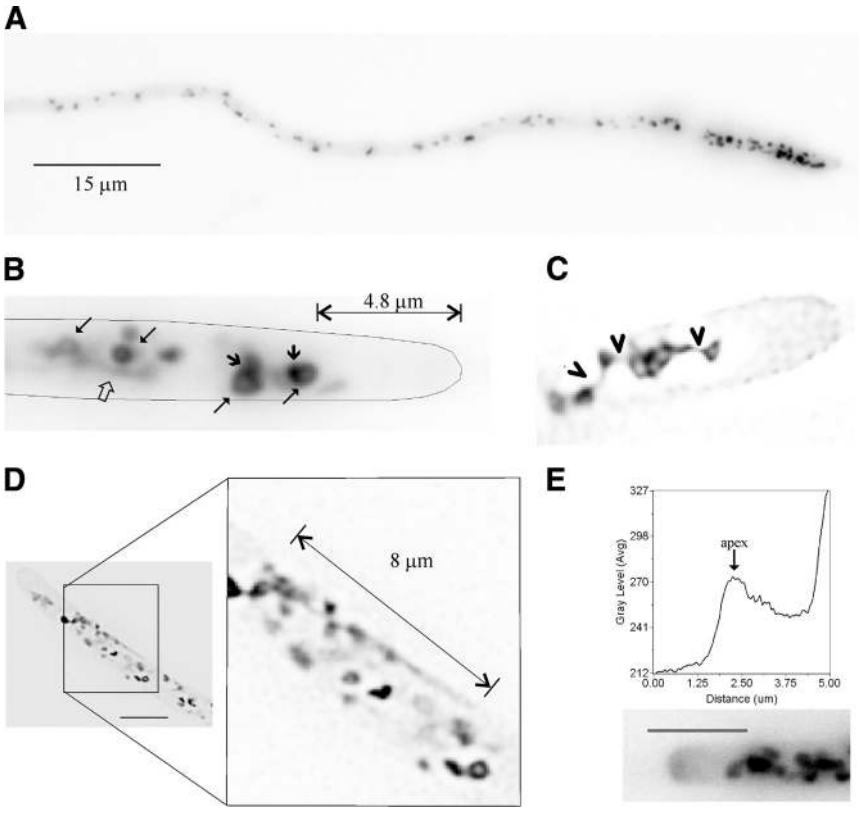

Figure 2. Organization, dynamics, and morphology of GEs labeled with mRFP-PH^{OSBP}. All images are shown in inverted contrast for clarity. (A) Polarization of GEs shown in a long hypha. The image is a maximal intensity projection of a z-stack series. (B) Ring-shaped structures (long arrows), accretions of stronger fluorescence (short arrows), and tubular extensions (open arrow) in the hyphal tip cell displayed in Supplemental Movie S1. The distance between the most apical, prominent Golgi body and the tip is indicated. (C) Deconvolved image showing a hyphal tip that contains a fenestrated structure connected to other polygonal structures by tubular extensions, which are indicated by arrowheads. (D) An example of a long tubular extension that connects a network of Golgi bodies. (E) A hyphal tip showing (in inverted contrast) a cloud of mRFP-PH^{OSBP} at the apical dome. A line scan is shown to illustrate the increase in fluorescence near the apex. Bar, 5 μm.

μm (Figure 2, C and D, and Supplemental Movie S1). In addition, fenestrated structures connected by tubules could clearly be seen in deconvolved images (Figure 2C). We conclude that the *A. nidulans* Golgi does not form stacks and involves a very dynamic network of tubules, rings, and fenestrated structures undergoing rapid changes in morphology. This network likely corresponds to the fenestrated sheets or ring structures with tubular projections seen in EM studies (Howard, 1981; Kurtz *et al*., 1994; see Bourett *et al*., 2007 for a review).

While individual Golgi bodies show short distance motility, the whole network of mRFP-PH^{OSBP} structures is highly dynamic and the fluorescence intensity of the structures changes rapidly with time, which occasionally gives the false impression of rapid movement (Supplemental Movies S1–S3). This possibly led others to conclude that GEs undergo rapid tip-directed movement (Hubbard and Kaminskyj, 2008). However, rapid movement of GEs could not be seen after careful inspection of a large number of time-lapse sequences made from frames taken every 1 to 10 s for >5 min. Moreover, the absence of long distance movement of GEs was unambiguously established using nuclei or early endosomes as landmarks (see below).

Golgi recruitment of the PH^{OSBP} domain is largely dependent on PtdIns4P, indicating that the Golgi membranes visualized with mRFP-PH^{OSBP} are *trans*-Golgi domains (Levine and Munro, 2002; Behnia and Munro, 2005). To confirm this prediction, we constructed a GFP-tagged version of *A. nidulans* Sec7, denoted HypB (Yang *et al*., 2008), because *S. cerevisiae* Sec7p is a prototypic resident of the *trans*-Golgi (Achstetter *et al*., 1988; Matsuura-Tokita *et al*., 2006; Losev *et al*., 2006). HypB^{Sec7}-GFP was expressed at physiological levels after gene replacement. Strains carrying this allele showed no growth defect, strongly indicating that the fusion protein is fully functional.

HypB^{Sec7}-GFP displays markedly lower levels of fluorescence than mRFP-PH^{OSBP}. Despite this relatively weak signal, rings, fenestrated structures, and tubules are nearly discernable in unprocessed images (not shown) and were clearly resolved after deconvolution. Time lapse movies revealed that these structures appear to undergo frequent exchange of membranes (Figure 3A and Supplemental Movie S4). As with mRFP-PH^{OSBP}, HypB^{Sec7}-GFP GEs show polarized distribution. Indeed HypB^{Sec7}-GFP colocalized with mRFP-PH^{OSBP} in live specimens (Figure 3B) and fixed cells (data not shown). We conclude that rings, fenestrated structures, and tubules genuinely represent the morphology of GEs at the resolution of the light microscope and that the *A. nidulans* membranes visualized with mRFP-PH^{OSBP} represent the *trans*-Golgi.

One important issue was determining the spatial relationship between the most apical *trans*-Golgi membranes and the plasma membrane at the apex, where secretion predominates (Taheri-Talesh *et al*., 2008). We observed that the relative distance of the most anterior mRFP-PH^{OSBP} GEs to the apex increases with the rate of apical extension, such that in rapidly growing tips (>0.5 μm/min at 25°C), this distance was as large as 5 μm (Supplemental Movies S1 and S2; Figure 2, B and C). In contrast, CopA$^{\alpha\text{-COP}}$ GEs are excluded from the apex-proximal 1 μm region (Breakspear *et al*., 2007). Because CopA$^{\alpha\text{-COP}}$ should, at least in part, localize to the early Golgi and as we show below that early Golgi membranes reach the apical dome, this difference possibly reflects the *trans*-Golgi–specificity of our reporter.

Within the subapical region devoid of *trans*-Golgi membranes, we could frequently visualize a haze of fluorescent material associated with the apical dome (Figure 2E). In appropriately contrasted time lapse movies, we could observe how clouds of mRFP-PH^{OSBP} membranes appear to detach from the most anterior GEs, reaching the plasma

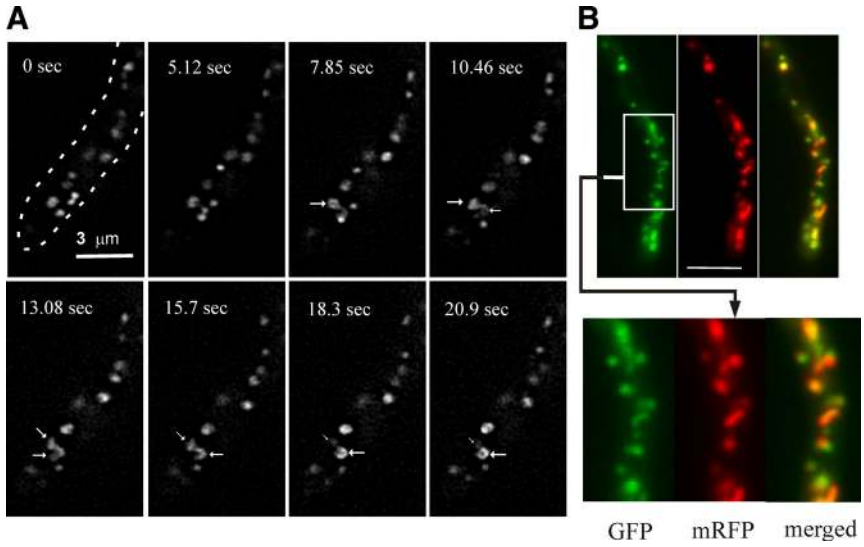

Figure 3. Dynamics of *trans*-Golgi equivalents as seen with HypB^{Sec7}-GFP and colocalization with mRFP-PH^{OSBP}. (A) The different panels, corresponding to Supplemental Movie S4, are projections of deconvolved z-stacks taken at the indicated time-points. The arrows indicate two connected ring-shaped structures, one of which appears to increase in fluorescence at the expense of the other. The arrow sizes have been increased or decreased with the relative intensity of their corresponding ring structures. (B) Colocalization of mRFP-PH^{OSBP} and HypB^{Sec7}-GFP. A strain carrying the transgenes expressing the two fluorescent reporters was photographed using GFP and mRFP specific filter sets. The two reporters overlap. Bar, 5 μm.

membrane of the apical dome (Supplemental Movie S3). We hypothesize that these clouds correspond to secretory tubules/vesicles arising from the *trans*-Golgi.

GE Polarization and Nuclear Distribution: GEs Are not Disassembled during Mitosis

A. nidulans apical cells are multinucleated. The region near the tip appears to play a major role in secretion because MTs associated with the first mitotic spindle do not disassemble in mitosis, ensuring that growth continues at normal rate (Horio and Oakley, 2005). Thus, we determined the intracellular distribution of the Golgi relative to nuclei labeled with the PacC^{27} transcription factor, which is exclusively nuclear during interphase (Mingot *et al*., 2001; Fernández-Martínez *et al*., 2003). We coimaged mRFP-PH^{OSBP} with GFP-PacC^{27} and quantified, in n = 9 apical cells, mRFP-PH^{OSBP} fluorescence in the region between the apex and the "leading" nucleus and in increasingly distal internuclear regions. This analysis demonstrated that GEs are strongly polarized ahead of the leading nucleus and that their relative density within a given internuclear region decreases with the distance to the tip (Figure 4, A and B). Previous work with *Candida albicans* established that GEs redistribute toward the growing tip during the yeast-to-hypha transition (Rida *et al*., 2006). Thus, we studied the polarization of *A. nidulans* GEs during germ-tube emergence. Figure 4C shows that GEs are randomly distributed in isotropically growing conidiospores. As soon as polarity is established, GEs migrate into the germ-tube primordium and polarize as the germtube undergoes apical extension. Golgi polarization occurs before the leading nucleus (arrowed) migrates into the germtube (Figure 4C).

During the "open" mitosis of mammalian cells, the nuclear envelope is completely disassembled and the Golgi undergoes complete fragmentation/cytoplasmic dispersion (Barr, 2004; Altan-Bonnet *et al*., 2006; Colanzi and Corda, 2007). In contrast, the Golgi remains intact during the *S. cerevisiae* "closed" mitosis (Preuss *et al*., 1992). Thus, the mitotic mammalian Golgi disassembly might be connected to the adjustments required by the ER after nuclear envelope breakdown.

In *A. nidulans*, the mitosis is closed but, in contrast to *S. cerevisiae*, the hyphal tip cell contains multiple nuclei whose nuclear pore complexes (NPCs) are disassembled at the onset of mitosis, allowing the nuclear entry of tubulin (De Souza *et al*., 2004). To address the fate of GEs during mitosis we used as direct criterion for mitotic entry/exit the release to the cytosol of a proportion of GFP-PacC^{27} [following NPC disassembly at G2/M, the fraction of PacC^{27} that is not DNA-bound is released to the cytosol (De Souza *et al*., 2004; Araujo-Bazán *et al*., 2008a)]. The nuclei enter mitosis in a nearly simultaneous manner, resulting in a conspicuous increase of cytosolic GFP-PacC^{27} fluorescence. Figure 5 (Supplemental Movie S5) shows two nuclei undergoing mitosis (frames 2, 3, and 4, note the increase in cytosolic GFP fluorescence compared with G2 [frame 1] or G1 [frames 5 and 6], after mitotic exit). Supplemental Figure S1 shows two nuclei captured in G2, prophase/metaphase, late anaphase, and telophase. No significant differences in Golgi organization or polarization were detectable throughout. We conclude that the *A. nidulans* Golgi remains intact during mitosis.

The Subcellular Distribution of ER Exit Sites

To address the possibility that polarization of Golgi cisternae reflects predominance of ER exit sites (ERES) in the tip region, we used the COPII coat component Sec23 as a prototypic marker of transitional ER (Rossanese *et al*., 1999). 771 residue *A. nidulans* Sec23 (AnSec23), corresponding to AN0261, shows 53% amino acid sequence identity to *S. cerevisiae* Sec23p. Thus, we constructed *sec23-gfp*, a gene-replacement allele expressing a C-terminal fusion of GFP to AnSec23. *sec23-gfp* strains grew somewhat slower than the wild-type, indicating that GFP attachment weakly impairs Sec23 function. However, conclusions on AnSec23-GFP localization were confirmed using a diploid (or aneuploid) strain serendipitously obtained by transformation, which carries a wild-type *sec23* allele in addition to *sec23-gfp* and showed no growth impairment. This led us to conclude that the localization described below is bona fide.

AnSec23-GFP localizes to a cytosolic haze and to numerous small fluorescent foci that are markedly more abundant than mRFP-PH^{OSBP} GEs. Although these foci are present across the entire length of the cells, they clearly predominate near the tips. This predominance is more conspicuous in rapidly growing hyphae than in more slowly growing germlings (Figure 6, A and B; Supplemental Figure S4). Fluorescence intensity analyses established that AnSec23 ERES are more abundant in the two internuclear regions nearest to the

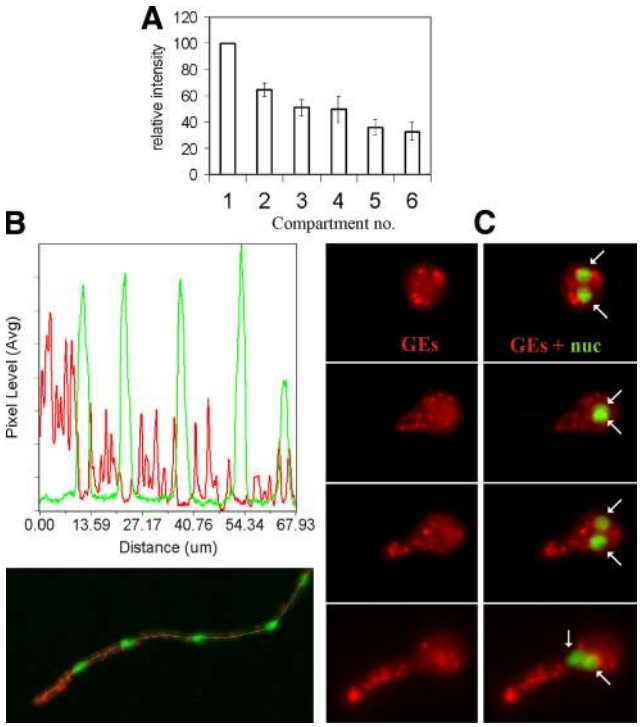

Figure 4. Polarization of GEs ahead of the leading nucleus. A strain coexpressing GFP-PacC^{27} and mRFP-PH^{OSBP} was photographed. (A) Maximal intensity projections of z-stack series of hyphal tip cells were used to define regions of interest in the area located ahead of the leading nucleus as well as in the internuclear regions. The average intensity in these regions was determined in n = 9 hyphal tip cells. The average fluorescence intensity of successive internuclear regions was plotted relative to that of the leading region. (B) Quantification of average pixel intensity in the red and green channels across the 8-pixel-wide line shown in the maximal intensity projection image, clearly illustrating polarization ahead of the leading nucleus. (C) GEs are randomly distributed during the isotropic growth phase and polarize to the growing apex as soon as polarity is established, before the leading nucleus migrates into the germtube. Panels in the left column show mRFP-PH^{OSBP} Golgi equivalents, whereas those in the right column show the same images merged with the GFP-PacC^{27} channel. The positions of two nuclei are indicated by arrows.

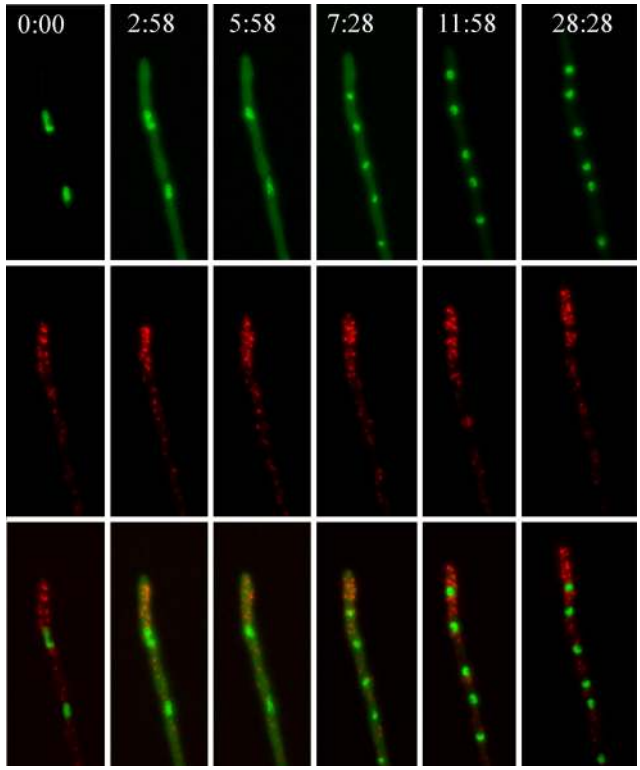

Figure 5. The Golgi is not disassembled during mitosis. The images shown are maximal intensity projections of z-stack series and correspond to frames from Supplemental Movie S5. Time is in min:sec. Note the cytosolic GFP fluorescence due to partial release of PacC^{27} from the nuclei to the cytosol during mitosis (second, third, and fourth time points).

tip (considering as the nearest the one located between the leading nucleus and the apex) than in more distal internuclear regions (Figure 6I). Moreover, AnSec23 foci clearly polarized into new tips emerging after reversal of LatB-mediated inhibition of apical extension (Supplemental Movie S15, see below). AnSec23 ERES are not excluded from the apex-proximal region, closely approaching the apical dome plasma membrane (Figure 6, A–D). As AnSec23-GFP foci do not colocalize with mRFP-PH^{OSBP} GEs, the lack of a region of exclusion of ERES near the apex is best illustrated in dual channel images of a strain coexpressing both markers (Figure 6D). Time-lapse movies revealed that foci undergo rapid short-distance pulsatory movements (Figure 6C) (Supplemental Movie S6).

Early Golgi Membranes also Show Polarization toward the Tip

GrhA (AN11248) is the *A. nidulans* orthologue of *S. cerevisiae* Grh1p. Grh1p contributes to the efficiency of tethering events in the early Golgi, where it is recruited via a conserved N-terminally acetylated amphipatic helix (Behnia *et al.*, 2007). We tagged GrhA with GFP in its C terminus by gene replacement. *grhA::gfp* strains showed no apparent growth defect. Figure 6, E–H shows that GrhA localizes to a cytosolic haze and to punctate structures that are less fluorescent and less abundant than those of Sec23-GFP (the lower abundance is noticeable by comparing the kymographs in Figure 6, C and F). Experiments described below showed that while AnSec23-GFP foci are not affected by brefeldin A (BFA), GrhA-containing membranes aggregate in the presence of the drug. This indicates that GrhA structures have Golgi features and establishes that GrhA and AnSec23 localize to different compartments. As BFA-sensitive GrhA structures do not colocalize with *trans*-Golgi elements (Figure 6H), we conclude that GrhA localizes to early Golgi membranes.

Like *trans*-Golgi elements, GrhA-GFP early Golgi structures are polarized (Figure 6, E, F, and I). In deconvolved z-stacks, some GrhA-GFP structures appear to be accretions within a network of fainter tubular structures (Figure 6G). Time-lapse movies (Supplemental Movie S7) showed that a major proportion of GrhA structures generally undergoes pulsatory short-distance movement similar to that of AnSec23-GFP foci. However, examples of GrhA-GFP structures that move for longer distances in either direction were not infrequent (Figure 6F), although this movement was clearly slower than that of early endosomes (see below). Importantly, GrhA structures are not excluded from the tip, where they nearly reach the actual apex (Figure 6H).

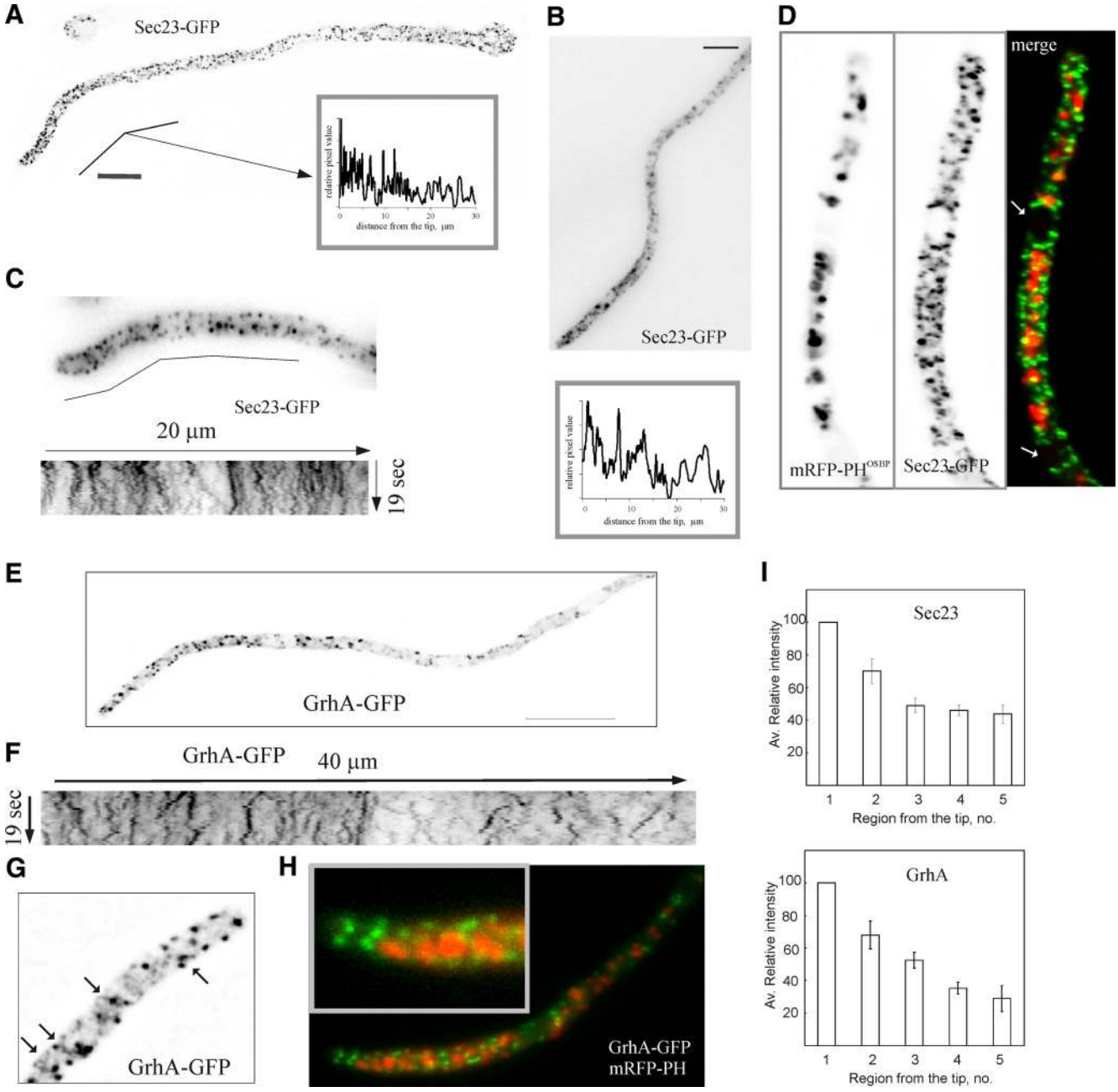

Figure 6. The subcellular localization and dynamics of early Golgi membranes and ERES. (A) Localization of ERES labeled with AnSec23-GFP in a germling. The image is a maximal intensity projection of a deconvolved z-stack series. Polarization is illustrated by the linescan in the insert. (B) Polarization of ERES in a hyphal tip. The image is a maximal intensity projection of a z-stack series. The line scan below, starting from the apex, demonstrates polarization. Bar, 5 μm. (C) Dynamics of AnSec23-GFP foci. The image corresponds to a time-lapse series made with frames taken every 500 msec. The kymograph shown below corresponds to the indicated 20-μm-long line. (D) Dual channel imaging of AnSec23-GFP and mRFP-PH^{OSBP} GEs. The arrows indicate the position of two nuclei. Note that AnSec23-GFP foci reach the apical dome. (E) Maximal intensity projection of a z-stack series illustrating polarization of GrhA-GFP punctate structures. Bar, 10 μm. (F) A kymograph illustrating the dynamics of GrhA-GFP structures across a 40-μm line that starts at the apex of the cell displayed in Supplemental Movie S7. For comparison, the kymograph is displayed at the same scale than that in C. (G) Single plane of a deconvolved z-stack series showing that GrhA-GFP appears to label accretions connected to a tubular network (examples indicated with arrows). (H) Dual channel imaging of GrhA-GFP and mRFP-PH^{OSBP} GEs. The inset shows how early but not *trans*-Golgi elements reach the apical dome. (I) Analyses of AnSec23-GFP and GrhA-GFP fluorescence. The average fluorescence intensity in the successive internuclear regions was determined and plotted relative to that measured in the region between the leading nucleus and the apex, which was set as 100% and considered as region no. 1. For AnSec23, the position of the nuclei in n = 10 rapidly growing hyphae was inferred because some ERES associate with the nuclear envelope (see D). For GrhA-GFP, the position of the nuclei in n = 14 hyphae was inferred from the regions of cytoplasmic fluorescence exclusion.

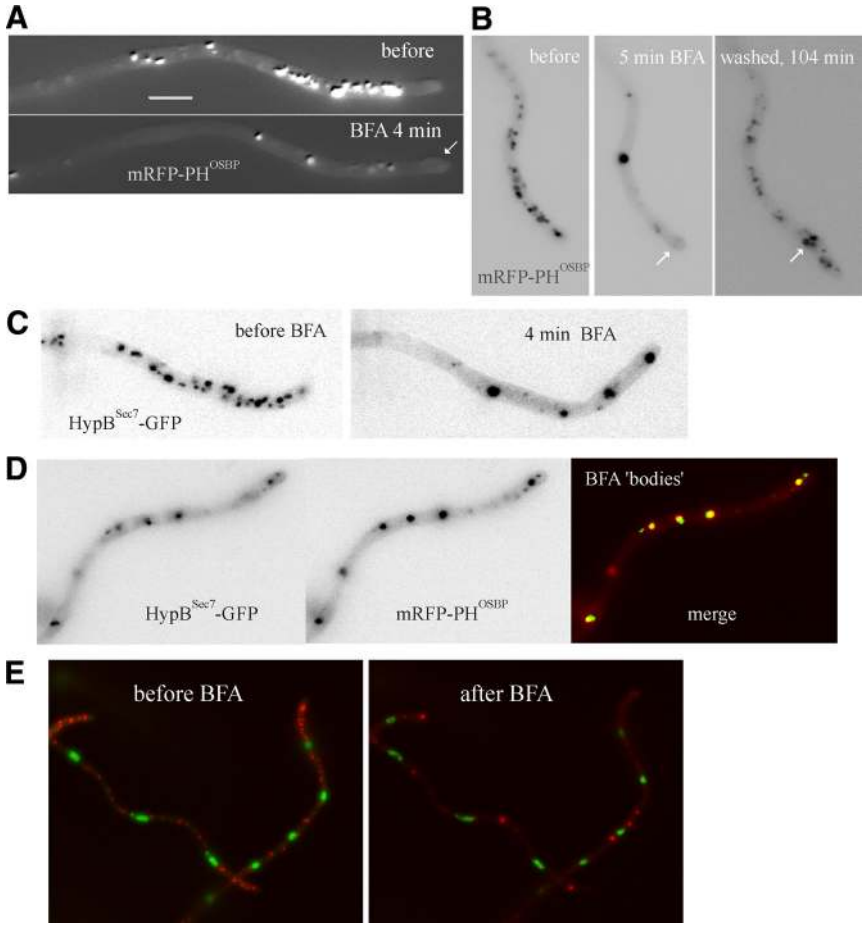

Figure 7. The effects of brefeldin A on the organization of the Golgi. (A) Maximal intensity projections of z-stack series (5 planes) of a hyphal tip cell expressing mRFP-PH^{OSBP}, before and after exposure to 300 μg/ml BFA. The projections were adjusted with the sharpening algorithm of Metamorph to improve visualization of GEs. (B) Recovery of the Golgi organization (determined with mRFP-PH^{OSBP}) after BFA washout. The images, corresponding to Supplemental Movie S8, are maximal intensity projections of z-stack series (each z-stack containing 3 planes, to minimize photodamage). In both A and B, arrows indicate swollen tips. (C) As in A, but the imaged strain expresses HypB^{Sec7}-GFP. Images are frames taken from Supplemental Movie S9. (D) Colocalization of mRFP-PH^{OSBP} and HypB^{Sec7}-GFP in brefeldin bodies. The experiment was carried out in the presence of 100 μg/ml BFA. (E) Brefeldin bodies are not associated with nuclei. A strain coexpressing GFP-PacC^{27} and mRFP-PH^{OSBP} was photographed before and after addition of BFA. The images are frames taken from Supplemental Movie S10.

Brefeldin A Reversibly Impairs A. nidulans *Apical Extension*

In mammalian cells (Lippincott-Schwartz *et al*., 1991; Sciaky *et al*., 1997) and in fungi (Rambourg *et al*., 1995a; Deitz *et al*., 2000, Rida *et al*., 2006), BFA leads to the disassembly of the Golgi. Therefore BFA was predicted to arrest *A. nidulans* apical extension.

We observed that *A. nidulans* conidiospore germination is not prevented by 300 μg/ml BFA, suggesting that the fungus is largely resistant. This was unexpected, because others reported effects on *A. nidulans* GEs of concentrations as low as 10 μg/ml (Hubbard and Kaminskyj, 2008). Thus, we investigated this apparent resistance further. We observed a significant drop in apical extension in 300 μg/ml BFA-treated germlings compared with mock-treated (with the BFA solvent DMSO) controls ($0.144 \pm 0.013\ \mu m \cdot min^{-1}$, n = 28 vs. $0.202 \pm 0.018\ \mu m \cdot min^{-1}$, n = 26; p = 0.0059), indicating that this high concentration of the drug, although clearly sublethal, impairs exocytic traffic. We next examined the effects of BFA on rapid apical extension in hyphae, where the strongest dependence on secretion was anticipated. Apical extension was largely decreased (100 μg/ml) or abolished (300 μg/ml) by BFA at 10 to 15 min after drug addition (data not shown and Supplemental Movies S8 to S12), correlating with slight tip swelling (Figure 7, A and B, arrows). However, growth in the presence of the drug was spontaneously and slowly resumed after ≈60 min (data not shown). Arrested tips resume normal growth after washing out BFA, indicating reversibility (Supplemental Movies S8 to S12). This critical control demonstrates that BFA-induced changes in the Golgi to be described below cannot be attributed to cell death. In view of the recovery seen after long incubation times in the presence of BFA, we restricted our observations to the early time points (always <40 min) after drug addition.

BFA Treatment Leads to Aggregation of Early and -trans-*Golgi Elements into Large Cytosolic Bodies*

mRFP-PH^{OSBP} *trans*-Golgi membranes underwent a dramatic reorganization very rapidly (1 to 2 min) after adding BFA, losing their polarized distribution and coalescing into a small number of characteristically larger fluorescent structures (brefeldin bodies; Figure 7, A and B; Supplemental Movie S8). Others, using GFP-CopA$^{\alpha\text{-COP}}$, did not observe BFA-induced aggregation of GEs and concluded instead that fewer GEs were observed after a very long (4 h) BFA treatment (Breakspear *et al*., 2007). In contrast, another report concluded, in agreement with our data, that BFA drives relocalization of the *A. nidulans* Arf1 orthologue ArfA^{Arf1} to aggregates after a 30 min incubation (Lee and Shaw, 2008). The GFP-CopA$^{\alpha\text{-COP}}$ study used agar plugs containing hyphae that were soaked in BFA-containing medium and did not include a washout control. Thus, slow drug diffusibility and/or cell stress resulting from this procedure might explain this apparently contradictory observation.

To further support our conclusions, we conducted similar studies using HypB^{Sec7}-GFP, which confirmed that loss of GE polarization, aggregation of Golgi bodies and subsequent wash-out-induced recovery were equally seen with this reporter (Figure 7C and Supplemental Movie S9). In-

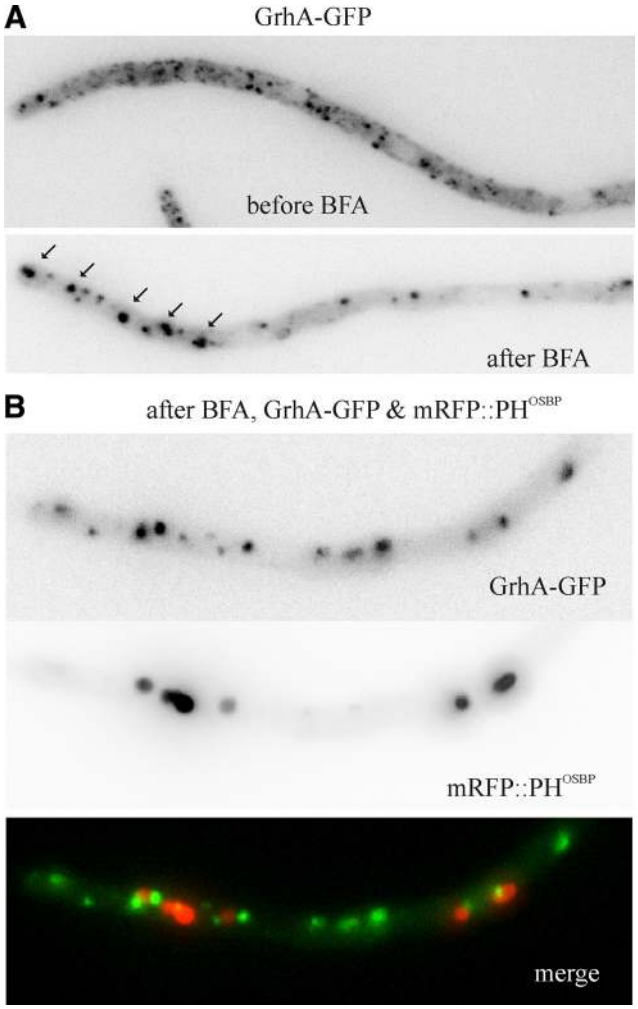

Figure 8. mRFP-PH^{OSBP} and GrhA-GFP Golgi membranes aggregate into different brefeldin bodies. (A) GrhA-GFP relocalizes to aggregates upon BFA treatment of cells only expressing this fluorescent reporter. (B) A hyphal tip cell of a strain coexpressing GrhA-GFP and mRFP-PH^{OSBP} reporters depicted after BFA treatment. Images correspond to a hyphal tip cell photographed at 25 min after BFA addition. The GFP and mRFP channels were acquired simultaneously using a DV2 Dual-View emission splitter. GrhA-GFP and mRFP-PH^{OSBP} aggregate into different bodies (see also Supplemental Movie S11).

deed HypB^{Sec7}-GFP and mRFP-PH^{OSBP} colocalized in the aggregates (Figure 7D). Thus, the *A. nidulans trans*-Golgi undergoes major changes but is not completely disorganized by BFA. The somewhat regular distribution of *trans*-Golgi BFA aggregates along the hyphal cells does not reflect association with the evenly spaced nuclei (Figure 7E; Supplemental Movie S10).

Using GrhA-GFP, we determined that early Golgi cisternae also aggregate in the presence of BFA (Figure 8A and Supplemental Movie S11), although this effect was somewhat less strong than that seen with mRFP-PH^{OSBP} or HypB^{Sec7}-GFP. Early Golgi recovery after washout is somewhat faster than that of the *trans-Golgi* (not shown). This aggregating effect of BFA is Golgi-specific as Sec23-GFP ERES were unaffected by the drug (Supplemental Figure S2; Supplemental Movie S12). Unexpectedly, although both early and *trans*-Golgi membranes form BFA-induced aggregates, strictly simultaneous dual channel imaging (using a Dual-View, see materials and Methods) revealed that the corresponding reporters localize to different brefeldin bodies (Figure 8 and Supplemental Movie S11), indicating that early and *trans*-Golgi membranes segregate spatially when the BFA target(s) is/are inhibited.

In every instance where recovery subsequent to BFA washout was filmed, the early and *trans*-Golgi organization was recovered before growth was resumed, strongly indicating that the normal organization of the Golgi is required for apical extension.

The Effects of Cytoskeletal Inhibitors on the Golgi and on Transitional ER

MTs are essential for rapid hyphal growth (Horio and Oakley, 2005; Taheri-Talesh *et al*., 2008). A previous report concluded, using nocodazol, that MTs do not have a major role in the polarization of Golgi equivalents (Breakspear *et al*., 2007). This study examined the effects of depolymerising MTs on GEs at a relatively late time point (2 h) after adding the drug, but no observations were made earlier; in addition, we examined ERES, early and *trans*-Golgi specific reporters, rather than α-COP.

We verified, using TubA (α-tubulin)-GFP, that addition of 5 μg/ml benomyl leads to the complete and reversible disassembly of microtubules within 10 min (Supplemental Figure S3, A–C), correlating with a sharp decrease of apical extension rate, often associated with tip bulging (Horio and Oakley, 2005; Taheri-Talesh *et al*., 2008). In benomyl-treated cells, mRFP-PH^{OSBP} GEs appeared to concentrate in the bulged tips, getting closer to the apical plasma membrane but maintaining their polarization ahead of the leading nucleus (Supplemental Figure S3). On benomyl washout, normal tips emerged from the bulged regions and GEs polarized into these tips as they underwent apical extension (Supplemental Movie S13). AnSec23-GFP ERES and GrhA-GFP membranes similarly concentrated in the bulged tips upon benomyl treatment and did not depolarize (Supplemental Figure S4). We note, however, that MTs help to position the F-actin dependent tip growth apparatus (Taheri-Talesh *et al*., 2008) and therefore these effects of benomyl could be indirect.

A previous study (Hubbard and Kaminskyj, 2008) addressed the role of F-actin in the dynamics of GFP-CopA *A. nidulans* GEs using a relatively low concentration of latrunculin B (5 μg/ml), which possibly results in incomplete disorganization of F-actin. However, the role of F-actin in the polarization of *A. nidulans* Golgi has not been analyzed in detail, nor has it been determined whether the Golgi morphology is dependent on the actin cytoskeleton. These studies are relevant because previous work established that GEs polarize in *Candida albicans* hyphae in an actin-dependent manner (Rida *et al*., 2006).

Thus we used latrunculin B at a concentration (40 μg/ml) that completely and reversibly disorganizes endocytic actin patches (Figure 9A). Within a few minutes after drug addition AbpA^{Abp1} patches were disassembled, growth stopped and hyphal tips underwent bulging as we reported previously (Taheri-Talesh *et al*., 2008; Araujo-Bazán *et al*., 2008b; Figure 9A). Growth was restored (frequently from "split tips") and endocytic patches reassembled 1 h after washing out the drug (Figure 9A). Latrunculin led to clear depolarization of mRFP-PH^{OSBP} GEs, despite the fact that the most anterior GEs appear to collapse against the bulged tips (Figure 9; compare C and D). In addition, the density of GEs per unit length increased significantly (0.92 ± 0.06 bodies/μm in $n = 10$ untreated tips vs. 1.58 ± 0.14 bodies/μm in $n = 10$ treated ones; $p = 0.001$), correlating with a ≈25% reduction

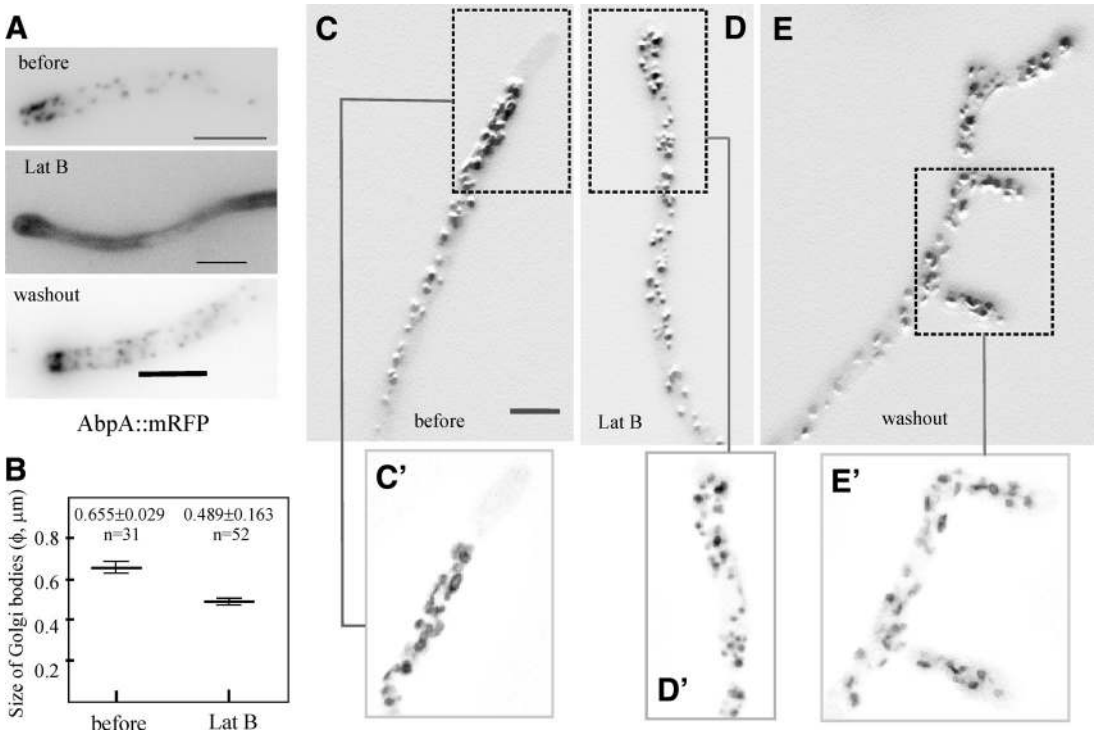

Figure 9. Involvement of F-actin in the organization and polarization of GEs. (A) Control experiment showing latrunculin B-mediated reversible disassembly of AbpA^{Abp1} patches. These patches, which are present across the complete length of the hyphae, form a prominent subapical ring (before). On latrunculin B treatment, these patches are disassembled and AbpA^{Abp1} becomes cytosolic. The latrunculin B (Lat B)-treated tip corresponds to a sample incubated for 12 min in the presence of 40 μg/ml latrunculin and is a maximal intensity projection of four z-planes. The tip shows the characteristic Lat B–induced apical swelling. At ≈1h after Lat B washout, apical growth was resumed and the subapical rings of AbpA^{Abp1} were reassembled. (B) The size of Golgi bodies is significantly lower ($p = 0.0001$) in the presence of Lat B. Statistical significance was determined using a two-tailed unpaired *t* test. (C) Polarization and organization of GEs before Lat B treatment. The upper image is a maximal intensity projection of a 7-image z-stack series. The boxed image below is a maximal intensity projection of the same planes after deconvolution. Note the characteristic irregular ring shaped structures connected by tubules. (D) Polarization and organization of GEs in the presence of 40 μg/ml Lat B. The image is a maximal intensity projection of a 5-image z-stack series and the boxed image below is a maximal intensity projection of the same planes after deconvolution. Note the smaller punctate appearance of GEs and their proximity to the bulged tip. (E) Repolarization of GEs after Lat B washout. The large image (a maximal intensity projection of a 5-image z-stack series) shows one example of a hypha in which growth was resumed from three nearly adjacent polarity axes. The picture was taken at 1 h after Lat B washout. It clearly shows how GEs predominate toward the region where the three new tips emerge and within the growing tips themselves. The boxed image is a maximal intensity projection of the same planes after deconvolution. Note how ring-shaped structures are clearly discernable near the tips. The images in C, D, and E are shown at the same magnification to facilitate comparison, with the bar in C representing 5 μm. The maximal intensity projections in the larger images were processed using the sharpen algorithm of Metamorph to improve visualization.

in their average size (Figure 9, B and D′). Finally, ring-shaped GEs were hardly resolved in deconvolved images of latrunculin-treated tips (Figure 9, compare panels C′ and D′), although this effect might just reflect the overall reduction in GE average size noted above (i.e., the central "hollow" area might fall below resolution). Washout experiments showed that the effect of latrunculin on the polarization of mRFP-PH^{OSBP} GEs was reversed one hour after removing the drug, coinciding with resumption of growth from split or bulged tips (Figure 9E; Supplemental Movie S14). GEs migrated into these new tips after the newly established polarity axes and ring-shaped GEs reappeared (Figure 9E′). We conclude that F-actin plays a role both in determining the morphology and the polarization of *trans*-Golgi membranes.

Similar experiments demonstrated that the polarization of AnSec23-GFP ERES is dependent on the actin cytoskeleton (Supplemental Figure S4). Time lapse microscopy showed that AnSec23 foci depolarized by latrunculin reconcentrated in the tips of the new polarity axes arising after drug washout (Supplemental Movie S15). Unfortunately, we were unable to establish any firm conclusion on the effects of latrunculin B on the distribution or morphology of GrhA-GFP membranes.

trans-Golgi Elements Are Relatively Static Compared with Early Endosomes and do not Reach the Dynein Loading Zone

One feature unequivocally distinguishing the Golgi and early endosomes is the absence of long-distance movement of GEs. GFP-RabA^{Rab5} early endosomes show rapid bidirectional movement on MTs tracks (Abenza *et al.*, 2009), contrasting with the relatively slow, short distance movement of mRFP-PH^{OSBP} Golgi equivalents (Figure 10, A and B; Supplemental Movie S16). Occasionally, early endosomes associate with GEs before or after undergoing movement. These data and the time-lapse sequences discussed above unequivocally demonstrate that GEs do not undergo rapid tip-directed movement, in disagreement with a previous report (Hubbard and Kaminskyj, 2008).

If NudA cytoplasmic dynein function is compromised, early endosomes form an exaggerated compartment near

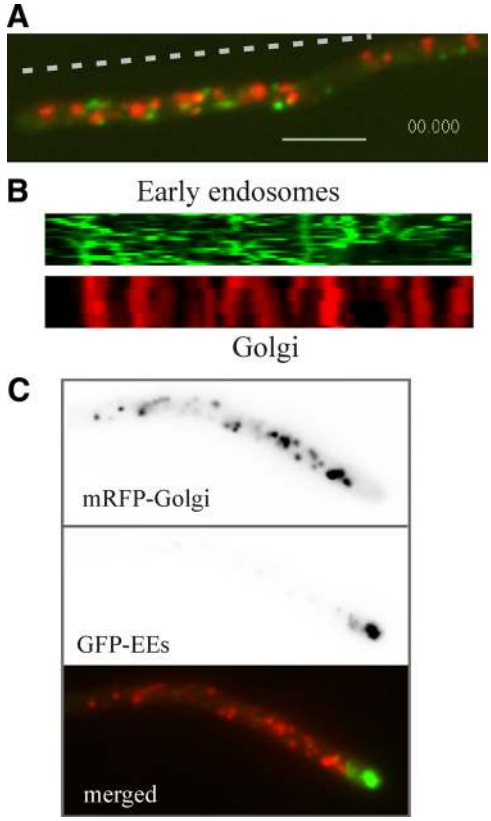

Figure 10. The relationship of the Golgi with early endosomes. (A) Still image corresponding to a single plane of Supplemental Movie S16, which illustrates the high motility of early endosomes labeled with GFP-RabA^{Rab5} compared with the relatively static GEs. Bar, 5 μm. (B) Kymographs along the dotted line indicated in A of the time series images in the GFP and mRFP channels. (C) The spatial relationship of the most apical GEs with the dynein loading zone. The images correspond to a *nudA1* cell incubated at 25°C and shifted to 42°C for 3.5 h.

the apex, at the region where the (+)-ends of MTs converge, because early endosomes traffic through this region before undergoing dynein-dependent retrograde movement (Lenz *et al*., 2006; Zekert and Fischer, 2008; Abenza *et al*., 2009). We determined the spatial relationship between the most apical *trans*-Golgi membranes and this exaggerated endosomal compartment by coimaging GFP-RabA^{Rab5} with mRFP-PH^{OSBP} in *kinA*Δ (data not shown) [the KinA kinesin delivers dynein to the (+)-ends of MTs (Zhang *et al*., 2003)] and *nudA1*^{ts} mutants. Both in *kinA*Δ and restrictive temperature-incubated *nudA1* mutants, showing moderate and strong enlargement of the early endosomal compartment at the tip, respectively, this compartment lies immediately behind the apex, ahead of the most apical *trans*-Golgi membranes, with which it does not overlap (Figure 10C).

DISCUSSION

This is the most detailed in vivo characterization of the Golgi reported so far in any filamentous fungus. Like in *S. cerevisiae* (Matsuura-Tokita *et al*., 2006; Losev *et al*., 2006), the *A. nidulans* Golgi visualized with fluorescent proteins is a dynamic network of ring and fenestrated structures connected by tubular extensions. The robust mRFP-PH^{OSBP} signal allowed visualization of ring and tubules of the *trans*-Golgi in untreated epifluorescence images. However, deconvolution was required for visualization of fenestrated structures and facilitated detection of ring-shaped cisternae with physiological levels of HypB^{Sec7}-GFP.

A. nidulans early Golgi membranes seen with GrhA-GFP are small discs that could not be resolved into rings, which might reflect either the relatively weak signal of this reporter or the fact that GrhA is recruited to discrete sites on membranes. As GrhA-GFP and mRFP-PH^{OSBP} do not colocalize, we conclude that *A. nidulans* early and -*trans*-Golgi cisternae can be resolved by conventional microscopy. Unlike GrhA membranes (see below), AnSec23-GFP ERES appear to be BFA-insensitive. AnSec23-GFP ERES appeared as numerous small foci, indicating that COPII vesicles bud at random from ER membranes. In this pattern of ERES organization, *A. nidulans* resembles *S. cerevisiae* rather than *Pichia pastoris*, which contains a few discrete ERES. Such discrete organization has been proposed to underlie the formation of coherent Golgi stacks resembling the mammalian Golgi (Rossanese *et al*., 1999). The absence of coherent stacks in *A. nidulans* agrees with this proposal.

The Polarization of the Golgi and the Tip Growth Apparatus

The *A. nidulans* hyphal tip contains a network of actin cables radiating from the apex-associated Spitzenkörper (Pearson *et al*., 2004; Hohmann-Marriott *et al*., 2006; Taheri-Talesh *et al*., 2008) and is populated by MTs. In current models (Harris *et al*., 2005; Taheri-Talesh *et al*., 2008; Abenza *et al*., 2009), secretory vesicle transport switches from MT-mediated to actin cable-mediated within the region of the tip. Endocytosis is spatially associated to apical secretion to facilitate endocytic recycling. Cytoskeletal components, lipid domains (Pearson *et al*., 2004), and endocytic patches act concertedly, conforming a functional unit that has been denoted the tip growth apparatus (Taheri-Talesh *et al*., 2008). *A. nidulans trans*-Golgi cisternae are randomly localized in isotropically growing conidia, redistribute toward the nascent tip as soon as polarity is established, and predominate in the region located ahead of the leading nucleus during hyphal apical extension, seemingly moving en bloc in anterograde direction, associated with the growing tip (Supplemental Movies S1 and S2). The dynein loading zone through which early endosomes circulate before undergoing retrograde movement lies ahead of the most anterior (apical) *trans*-GEs. This arrangement is ideally suited to facilitate recycling of endocytic cargoes internalized in the subapical endocytic ring, which can travel retrogradely on dynein-powered endosomes to reach the most anterior GEs before returning to the plasma membrane via secretion.

An important question is what determines polarization of the *trans*-Golgi. The observations that AnSec23 and GrhA structures are also polarized suggest that, at least to a certain extent, the polarization of the *trans*-Golgi reflects the distribution of ERES and early Golgi compartments, but do not rule out other possibilities. In *S. cerevisiae*, *trans*-GEs concentrate into the polarized nascent bud by an actin cable-dependent mechanism (Rossanese *et al*., 2001). Septin and F-actin dependent polarization of GEs has also been demonstrated in *C. albicans* hyphae (Rida *et al*., 2006). Thus, it is tempting to speculate that polarization of *A. nidulans* ERES and *trans*-GEs involves actin cables radiating from the apex-associated SepA formin (Pearson *et al*., 2004).

LatB leads to fragmentation and depolarization of *trans*-Golgi GEs and to depolarization of ERES. BFA promotes the aggregation of early and *trans*-Golgi membranes. Both drugs arrest apical extension. In every instance examined, resump-

tion of growth after washout correlated with reacquisition of the normal polarization or morphology of these compartments, which underscores the crucial role that secretion plays in hyphal apical extension.

Whereas *A. nidulans trans*-Golgi membranes are absent from a 3–5 μm region behind the apex, ERES and early Golgi cisternae reach the apical dome. Thus, there might be a mechanism that specifically mediates retrieval of *trans*-Golgi cisternae inappropriately reaching the apical dome, perhaps corresponding to retrograde movements of mRFP-PH^{OSBP} membranes that we observed at the apical edge of the *trans*-Golgi (Supplemental Movies S1–S3). We speculate that this retrograde transport is dynein-mediated, resembling the dynein-mediated movement of Golgi cisternae toward the centrosome that determines their perinuclear localization in mammalian cells (Corthesy-Theulaz *et al*., 1992; Vaughan *et al*., 2002).

The Brefeldin Bodies

Like *A. nidulans*, *S. cerevisiae* is largely insensitive to BFA (Graham *et al*., 1993). In hypersensitive *S. cerevisiae erg6* mutants, BFA leads to the formation of abnormal spheroids ("brefeldin organelles"; Rambourg *et al*., 1995a; Deitz *et al*., 2000). The organization of the wild-type *A. nidulans* Golgi is dramatically perturbed by BFA. Within 2 to 5 min of treatment, apical extension is dramatically slowed or even completely arrested, hyphal tips undergo a characteristic swelling and early and *trans*-Golgi membranes lose their polarization, forming large aggregates (brefeldin bodies).

Notably, whereas *trans*-Golgi markers HypB^{Sec7}-GFP and mRFP-PH^{OSBP} colocalize in the same BFA aggregates, these are different from those formed by GrhA-GFP (early Golgi) membranes, demonstrating that these reporters label different Golgi domains. These data would be consistent with BFA acting at two different levels. In *S. cerevisiae*, BFA targets the Sec7 domain-containing Arf GEFs Gea1/Gea2p and Sec7p (Peyroche *et al*., 1999), acting at early and *trans*-Golgi cisternae, respectively.

ACKNOWLEDGMENTS

We thank Tim Levine (Institute of Ophthalmology, London, United Kingdom) and María Molina (Universidad Complutense, Madrid, Spain) for PH domain constructs, two anonymous referees and the Monitoring Editor for useful suggestions, and Herb Arst and Joan Tilburn for critical reading of the manuscript. This work was supported by DGICYT Grant BIO2006-0556 (to M.A.P.) and by a F.E.B.S. postdoctoral fellowship (to A.P.).

REFERENCES

Abenza, J. F., Pantazopoulou, A., Rodríguez, J. M., Galindo, A., and Peñalva, M. A. (2009). Long-distance movement of *Aspergillus nidulans* early endosomes on microtubule tracks. Traffic *10*, 57–75.

Achstetter, T., Franzusoff, A., Field, C., and Schekman, R. (1988). SEC7 encodes an unusual, high molecular weight protein required for membrane traffic from the yeast Golgi apparatus. J. Biol. Chem. *263*, 11711–11717.

Altan-Bonnet, N., Sougrat, R., Liu, W., Snapp, E. L., Ward, T., and Lippincott-Schwartz, J. (2006). Golgi inheritance in mammalian cells is mediated through endoplasmic reticulum export activities. Mol. Biol. Cell *17*, 990–1005.

Araujo-Bazán, L., Fernández-Martínez, J., Ríos, V. M., Etxebeste, O., Albar, J. P., Peñalva, M. A., and Espeso, E. A. (2008a). NapA and NapB are the *Aspergillus nidulans* Nap/SET family members and NapB is a nuclear protein specifically interacting with importin alpha. Fungal. Genet. Biol. *45*, 278–291.

Araujo-Bazán, L., Peñalva, M. A., and Espeso, E. A. (2008b). Preferential localization of the endocytic internalization machinery to hyphal tips underlies polarization of the actin cytoskeleton in *Aspergillus nidulans*. Mol. Microbiol. *67*, 891–905.

Barr, F. A. (2004). Golgi inheritance: shaken but not stirred. J. Cell Biol. *164*, 955–958.

Behnia, R., Barr, F. A., Flanagan, J. J., Barlowe, C., and Munro, S. (2007). The yeast orthologue of GRASP65 forms a complex with a coiled-coil protein that contributes to ER to Golgi traffic. J. Cell Biol. *176*, 255–261.

Behnia, R., and Munro, S. (2005). Organelle identity and the signposts for membrane traffic. Nature *438*, 597–604.

Béthune, J., Wieland, F., and Moelleken, J. (2006). COPI-mediated transport. J. Membr. Biol. *211*, 65–79.

Bourett, T. M., James, S. W., and Howard, R. J. (2007). The Endomembrane System of the Fungal Cell. In: Biology of the Fungal Cell, 2nd Edition, ed. R.J. Howard, N.A.R. Gow, Berlin: Springer-Verlag, 1–47.

Breakspear, A., Langford, K. J., Momany, M., and Assinder, S. J. (2007). CopA:GFP localizes to putative Golgi equivalents in *Aspergillus nidulans*. FEMS Microbiol. Lett. *277*, 90–97.

Calcagno-Pizarelli, A. M., *et al*. (2007). Establishment of the ambient pH signaling complex in *Aspergillus nidulans*: PalI assists plasma membrane localization of PalH. Eukaryot. Cell *6*, 2365–2375.

Clutterbuck, A. J. (1993). *Aspergillus nidulans*. In: Genetic Maps. Locus Maps of Complex Genomes, ed. S. J. O'Brien, Cold Spring Harbor: Cold Spring Harbor Laboratory Press, 3.71–3.84.

Colanzi, A., and Corda, D. (2007). Mitosis controls the Golgi and the Golgi controls mitosis. Curr. Opin. Cell Biol. *19*, 386–393.

Corthesy-Theulaz, I., Pauloin, A., and Pfeffer, S. R. (1992). Cytoplasmic dynein participates in the centrosomal localization of the Golgi complex. J. Cell Biol. *118*, 1333–1345.

De Souza, C. P., Osmani, A. H., Hashmi, S. B., and Osmani, S. A. (2004). Partial nuclear pore complex disassembly during closed mitosis in Aspergillus nidulans. Curr. Biol. *14*, 1973–1984.

Deitz, S. B., Rambourg, A., Kepes, F., and Franzusoff, A. (2000). Sec7p directs the transitions required for yeast Golgi biogenesis. Traffic *1*, 172–183.

Fernández-Martínez, J., Brown, C. V., Díez, E., Tilburn, J., Arst, H. N., Jr., Peñalva, M. A., and Espeso, E. A. (2003). Overlap of nuclear localisation signal and specific DNA binding residues within the zinc finger domain of PacC. J. Mol. Biol. *334*, 667–684.

Fuchs, U., Hause, G., Schuchardt, I., and Steinberg, G. (2006). Endocytosis is essential for pathogenic development in the corn smut fungus *Ustilago maydis*. Plant Cell *18*, 2066–2081.

Galindo, A., Hervás-Aguilar, A., Rodríguez-Galán, O., Vincent, O., Arst, H. N., Jr., Tilburn, J., and Peñalva, M. A. (2007). PalC, one of two Bro1 domain proteins in the fungal pH signaling pathway, localizes to cortical structures and binds Vps32. Traffic *8*, 1346–1364.

Graham, T. R., Scott, P. A., and Emr, S. D. (1993). Brefeldin A reversibly blocks early but not late protein transport steps in the yeast secretory pathway. EMBO J. *12*, 869–877.

Harris, S. D., Read, N. D., Roberson, R. W., Shaw, B., Seiler, S., Plamann, M., and Momany, M. (2005). Polarisome meets spitzenkorper: microscopy, genetics, and genomics converge. Eukaryot. Cell *4*, 225–229.

Higuchi, Y., Shoji, J. Y., Arioka, M., and Kitamoto, K. (2009). Endocytosis is crucial for cell polarity and apical membrane recycling in the filamentous fungus *Aspergillus oryzae*. Eukaryot. Cell *8*, 37–46.

Hohmann-Marriott, M. F., Uchida, M., van de Meene, A. M., Garret, M., Hjelm, B. E., Kokoori, S., and Roberson, R. W. (2006). Application of electron tomography to fungal ultrastructure studies. New Phytol. *172*, 208–220.

Horio, T., and Oakley, B. R. (2005). The role of microtubules in rapid hyphal tip growth of *Aspergillus nidulans*. Mol. Biol. Cell *16*, 918–926.

Howard, R. J. (1981). Ultrastructural analysis of hyphal tip cell growth in fungi: Spitzenkörper, cytoskeleton and endomembranes after freeze-substitution. J. Cell Sci. *48*, 89–103.

Hubbard, M. A., and Kaminskyj, S. G. (2008). Rapid tip-directed movement of Golgi equivalents in growing *Aspergillus nidulans* hyphae suggests a mechanism for delivery of growth-related materials. Microbiology *154*, 1544–1553.

Jackson, C. L. (2009). Mechanisms of transport through the Golgi complex. J. Cell Sci. *122*, 443–452.

Jackson-Hayes, L., Hill, T. W., Loprete, D. M., Fay, L. M., Gordon, B. S., Nkashama, S. A., Patel, R. K., and Sartain, C. V. (2008). Two GDP-mannose transporters contribute to hyphal form and cell wall integrity in *Aspergillus nidulans*. Microbiology *154*, 2037–2047.

Kurtz, M. B., Heath, I. B., Marrinan, J., Dreikorn, S., Onishi, J., and Douglas, C. (1994). Morphological effects of lipopeptides against *Aspergillus fumigatus* correlate with activities against (1,3)-beta-D-glucan synthase. Antimicrob. Agents Chemother. *38*, 1480–1489.

Lee, S. C., Schmidtke, S. N., Dangott, L. J., and Shaw, B. D. (2008). Aspergillus nidulans ArfB plays a role in endocytosis and polarized growth. Eukaryot. Cell *7*, 1278–1288.

Lee, S. C., and Shaw, B. D. (2008). Localization and function of ADP ribosylation factor A in *Aspergillus nidulans*. FEMS Microbiol. Lett. *283*, 216–222.

Lenz, J. H., Schuchardt, I., Straube, A., and Steinberg, G. (2006). A dynein loading zone for retrograde endosome motility at microtubule plus-ends. EMBO J. *25*, 2275–2286.

Levine, T. P., and Munro, S. (2002). Targeting of Golgi-specific pleckstrin homology domains involves both PtdIns 4-kinase-dependent and -independent components. Curr. Biol. *12*, 695–704.

Lippincott-Schwartz, J., Yuan, L., Tipper, C., Amherdt, M., Orci, L., and Klausner, R. D. (1991). Brefeldin A's effects on endosomes, lysosomes, and the TGN suggest a general mechanism for regulating organelle structure and membrane traffic. Cell *67*, 601–616.

Losev, E., Reinke, C. A., Jellen, J., Strongin, D. E., Bevis, B. J., and Glick, B. S. (2006). Golgi maturation visualized in living yeast. Nature *441*, 1002–1006.

Matsuura-Tokita, K., Takeuchi, M., Ichihara, A., Mikuriya, K., and Nakano, A. (2006). Live imaging of yeast Golgi cisternal maturation. Nature *441*, 1007–1010.

Mingot, J. M., Espeso, E. A., Díez, E., and Peñalva, M. A. (2001). Ambient pH signaling regulates nuclear localization of the *Aspergillus nidulans* PacC transcription factor. Mol. Cell. Biol. *21*, 1688–1699.

Mingot, J. M., *et al*. (1999). Specificity determinants of proteolytic processing of *Aspergillus* PacC transcription factor are remote from the processing site, and processing occurs in yeast if pH signalling is bypassed. Mol. Cell. Biol. *19*, 1390–1400.

Momany, M. (2002). Polarity in filamentous fungi: establishment, maintenance and new axes. Curr. Opin. Microbiol. *5*, 580–585.

Patterson, G. H., Hirschberg, K., Polishchuk, R. S., Gerlich, D., Phair, R. D., and Lippincott-Schwartz, J. (2008). Transport through the Golgi apparatus by rapid partitioning within a two-phase membrane system. Cell *133*, 1055–1067.

Pearson, C. L., Xu, K., Sharpless, K. E., and Harris, S. D. (2004). MesA, a novel fungal protein required for the stabilization of polarity axes in *Aspergillus nidulans*. Mol. Biol. Cell *15*, 3658–3672.

Peñalva, M. A. (2005). Tracing the endocytic pathway of *Aspergillus nidulans* with FM4–64. Fungal Genet. Biol. *42*, 963–975.

Peyroche, A., Antonny, B., Robineau, S., Acker, J., Cherfils, J., and Jackson, C. L. (1999). Brefeldin A acts to stabilize an abortive ARF-GDP-Sec7 domain protein complex: involvement of specific residues of the Sec7 domain. Mol. Cell *3*, 275–285.

Preuss, D., Mulholland, J., Franzusoff, A., Segev, N., and Botstein, D. (1992). Characterization of the *Saccharomyces* Golgi complex through the cell cycle by immunoelectron microscopy. Mol. Biol. Cell *3*, 789–803.

Punt, P. J., Dingemanse, M. A., Kuyvenhoven, A., Soede, R.D.M., Pouwels, P. H., and van den Hondel, C. A. M. J. J. (1990). Functional elements in the promoter region of the *Aspergillus nidulans gpdA* gene encoding glyceraldehyde-3-phosphate dehydrogenase. Gene *93*, 101–109.

Rambourg, A., Clermont, Y., Jackson, C. L., and Kepes, F. (1995a). Effects of brefeldin A on the three-dimensional structure of the Golgi apparatus in a sensitive strain of *Saccharomyces cerevisiae*. Anat. Rec. *241*, 1–9.

Rambourg, A., Clermont, Y., and Kepes, F. (1993). Modulation of the Golgi apparatus in *Saccharomyces cerevisiae sec7* mutants as seen by three-dimensional electron microscopy. Anat. Rec. *237*, 441–452.

Rambourg, A., Clermont, Y., Ovtracht, L., and Kepes, F. (1995b). Three-dimensional structure of tubular networks, presumably Golgi in nature, in various yeast strains: a comparative study. Anat. Rec. *243*, 283–293.

Rambourg, A., Jackson, C. L., and Clermont, Y. (2001). Three dimensional configuration of the secretory pathway and segregation of secretion granules in the yeast *Saccharomyces cerevisiae*. J. Cell Sci. *114*, 2231–2239.

Rida, P.C.G., Nishikawa, A., Won, G. Y., and Dean, N. (2006). Yeast-to-hyphal transition triggers formin-dependent Golgi localization to the growing tip in *Candida albicans*. Mol. Biol. Cell *17*, 4364–4378.

Rossanese, O. W., Reinke, C. A., Bevis, B. J., Hammond, A. T., Sears, I. B., O'Connor, J., and Glick, B. S. (2001). A role for actin, Cdc1p, and Myo2p in the inheritance of late Golgi elements in *Saccharomyces cerevisiae*. J. Cell Biol. *153*, 47–62.

Rossanese, O. W., Soderholm, J., Bevis, B. J., Sears, I. B., O'Connor, J., Williamson, E. K., and Glick, B. S. (1999). Golgi structure correlates with transitional endoplasmic reticulum organization in *Pichia pastoris* and *Saccharomyces cerevisiae*. J. Cell Biol. *145*, 69–81.

Sciaky, N., Presley, J., Smith, C., Zaal, K. J., Cole, N., Moreira, J. E., Terasaki, M., Siggia, E., and Lippincott-Schwartz, J. (1997). Golgi tubule traffic and the effects of brefeldin A visualized in living cells. J. Cell Biol. *139*, 1137–1155.

Stefan, C. J., Audhya, A., and Emr, S. D. (2002). The yeast synaptojanin-like proteins control the cellular distribution of phosphatidylinositol (4,5)-bisphosphate. Mol. Biol. Cell *13*, 542–557.

Steinberg, G. (2007). On the move: endosomes in fungal growth and pathogenicity. Nat. Rev. Microbiol. *5*, 309–316.

Szewczyk, E., Nayak, T., Oakley, C. E., Edgerton, H., Xiong, Y., Taheri-Talesh, N., Osmani, S. A., and Oakley, B. R. (2006). Fusion PCR and gene targeting in *Aspergillus nidulans*. Nat. Protoc. *1*, 3111–3120.

Taheri-Talesh, N., Horio, T., Araujo-Bazán, L., Dou, X., Espeso, E. A., Peñalva, M. A., Osmani, S. A., and Oakley, B. R. (2008). The tip growth apparatus of *Aspergillus nidulans*. Mol. Biol. Cell *19*, 1439–1449.

Tilburn, J., Scazzocchio, C., Taylor, G. G., Zabicky-Zissman, J. H., Lockington, R. A., and Davies, R. W. (1983). Transformation by integration in *Aspergillus nidulans*. Gene *26*, 205–211.

Upadhyay, S., and Shaw, B. D. (2008). The role of actin, fimbrin and endocytosis in growth of hyphae in *Aspergillus nidulans*. Mol. Microbiol. *68*, 690–705.

Valdez-Taubas, J., and Pelham, H. R. (2003). Slow diffusion of proteins in the yeast plasma membrane allows polarity to be maintained by endocytic cycling. Curr. Biol. *13*, 1636–1640.

Vaughan, P. S., Miura, P., Henderson, M., Byrne, B., and Vaughan, K. T. (2002). A role for regulated binding of $p150^{Glued}$ to microtubule plus ends in organelle transport. J. Cell Biol. *158*, 305–319.

Wedlich-Soldner, R., Straube, A., Friedrich, M. W., and Steinberg, G. (2002). A balance of KIF1A-like kinesin and dynein organizes early endosomes in the fungus *Ustilago maydis*. EMBO J. *21*, 2946–2957.

Yang, Y., El Ganiny, A. M., Bray, G. E., Sanders, D. A. R., and Kaminskyj, S. G. W. (2008). Aspergillus nidulans hypB encodes a Sec7-domain protein important for hyphal morphogenesis. Fungal Genet. Biol. *45*, 749–759.

Zekert, N., and Fischer, R. (2008). The *Aspergillus nidulans* kinesin-3 UncA motor moves vesicles along a subpopulation of microtubules. Mol. Biol. Cell *20*, 673–684.

Zhang, J., Li, S., Fischer, R., and Xiang, X. (2003). Accumulation of cytoplasmic dynein and dynactin at microtubule plus ends in *Aspergillus nidulans* is kinesin dependent. Mol. Biol. Cell *14*, 1479–1488.